Propeller at High Incidence

JOHN DE YOUNG*
Grumman Aircraft Engineering Corporation, Bethpage, N. Y.

Existing small-incidence theory is generalized by use of a propeller solidity based on an average blade chord. With this solidity, simple expressions are developed for sixteen possible derivatives such as propeller normal (or side) force. In addition, an expression is derived which indicates that the ratio of normal force at high incidence to normal force slope at zero inflow equals the tangent of the angle of incidence, provided that both quantities have equal advance ratios as determined from the velocity normal to the propeller disk. Thrust, torque, and power at high incidence are likewise derived as ratios to the zero incidence value. Except for a small dependence on solidity, these ratios are independent of propeller geometry. Good correlation is shown with experimental thrust and power ratios to an incidence of 85°.

Nomenclature

A = wing aspect ratio (b^2/S)
a = incremental slip-stream velocity at propeller disk
a_0 = blade section lift-curve slope/rad
B = number of blades
b = wing span, ft
b' = propeller blade chord, ft
$b'_{0.25, 0.5, \ldots}$ = blade chord at $(r/R) = 0.25, 0.50, \ldots$, ft
C_D = blade drag coefficient
$C_{L\alpha}$ = wing lift-curve slope $\{[d\,(\text{lift})/d\alpha]/qS\}$/rad
$C_{l'_{p'}}$ = wing damping-in-roll derivative $\{[d\,(\text{rolling moment})/d\,(pD/2V)]/qS'D\}$
$C_{m'}$ = pitching moment coefficient (pitching moment/$qS'D$)
C_m = [pitching moment/$\rho n^2D^5 = (\pi J^2/8)C_{m'}$]
ΔC_{mP} = increment in pitching moment due to direct forces on propeller; does not include slip-stream downwash on horizontal tail (change in pitching moment/$qS\bar{c}$)
C_N = normal force coefficient (normal force/qS')
C_N = [normal force/$\rho n^2D^4 = (\pi J^2/8)C_{N'}$]
$C_{n'}$ = yawing moment coefficient (yawing moment/$qS'D$)
C_n = [yawing moment/$\rho n^2D^5 = (\pi J^2/8)C_{n'}$]
ΔC_{nP} = increment in yawing moment due to direct forces on propeller: does not include slip-stream sidewash on vertical tail (change in yawing moment /qSb)
C_T = thrust coefficient [thrust/$\rho n^2D^4 = (\pi J^2/8)T_{c'}$] (thrust force/$qS'$)
$C_{Y'}$ = side-force coefficient (side force/qS')
C_Y = [side force/$\rho n^2D^4 = (\pi J^2/8)C_{Y'}$]
$\bar{c}$ = mean aerodynamic chord of wing, ft
c_r = root chord of wing, ft
D = propeller diameter, ft
f = thrust factor [Eq. (7) or (8)]
i_T = tilt of propeller thrust axis, measured relative to wing zero-lift angle, positive upward, rad
J = advance ratio (V/nD)
J_{0T} = advance ratio at zero thrust, $\alpha + i_T = 0$
J_{0P} = advance ratio at zero power, $\alpha + i_T = 0$
l_1 = distance from c.g. to propeller plane, parallel to thrust axis, positive forward, ft
M = freestream Mach number
N = propeller normal force, lb
n = propeller rotational speed, rps; or yaw moment, ft-lb
q = freestream dynamic pressure ($\rho V^2/2$), psf
R = propeller radius, ft
r = radius to blade element, ft
r' = dimensionless radial distance (r/R)
S = wing area, ft²
S' = propeller area (πR^2), ft²
T = propeller thrust, lb
$T_{c'}$ = thrust coefficient [thrust/$qS' = (8/\pi J^2)C_T$]
x = longitudinal coordinate measured positive forward of wing leading edge, ft
Δx = longitudinal change in neutral point or in a.c. due to direct propeller forces, ft
y = lateral coordinate measured positive to right of plane of symmetry, ft
Δy = lateral distance from thrust axis of one propeller to blade element of another, ft
V = freestream velocity, fps
z = distance from c.g. to thrust axis, positive downward, ft
α = wing angle of attack measured from zero lift, deg or rad
α_{in} = inflow angle at propeller disk [Eq. (11)], rad
α_{fuso} = angle between fuselage axis and wing α, positive upward, rad
β = blade angle at $0.75R$ relative to reference chord, plus 5° from zero-lift chord [Eq. (43)], deg
β_0 = blade angle at $0.75R$ for zero lift
ϵ = induced upwash, positive downward, rad
σ = propeller solidity, ratio of blade element area to annulus area at $0.75R$ $(4B/3\pi)(b'_{0.75}/D)$
σ_e = effective solidity $(\bar{b}'\sigma/b'_{0.75})$[Eq. (15)]
ψ = yaw angle of thrust axis

Subscripts and superscripts

α_{in} = differentiation with respect to inflow angle, α_{in}
ψ = differentiation with respect to yaw angle, ψ
r' = differentiation with respect to yawing velocity, $rD/2V$
q' = differentiation with respect to pitching velocity $qD/2V$
p' = differentiation with respect to rolling velocity $pD/2V$
0.75 = three-quarter propeller radius
P = power-on value
( )′ = value to the propeller, coefficients per unit disk area S'
$L.75$ = left blade position at three-quarters radius point
$R.75$ = right blade position at three-quarter radius point
w = wing
fus = fuselage
slip = propeller slip stream

Propeller derivatives for stability or flutter predictions

Z = -normal force, $\theta = \alpha$, $C_{Z'} = -C_{N'}$
$\pm$ = positive for clockwise propeller rotation, negative for anticlockwise
$\mp$ = negative for clockwise propeller rotation, positive for anticlockwise

All force coefficients are for unit $\frac{1}{2}\rho V^2S'$; all moment coefficients are for unit $\frac{1}{2}\rho V^2S'D$. In terms of the evaluated derivatives of Table 1,

$C_{Z'_\theta}(\delta) = -C_{Y'_\psi}\cos\delta_f$
$C_{Z'_\psi}(\delta) = \pm C_{Y'_\psi}\sin\delta_f$

Presented as Preprint 64-169 at the AIAA General Aviation Aircraft Design and Operations Meeting, Wichita, Kansas, May 25–27, 1964; revision received October 9, 1964.

* Theoretical Aerodynamicist.

$$
\begin{aligned}
C_{Z'_{q'}}(\delta) &= C_{Y'_{q'}} \sin\delta_f \\
C_{Z'_{r'}}(\delta) &= \pm C_{Y'_{q'}} \cos\delta_f \\
C_{Y'_{\theta}}(\delta) &= -C_{Z_{\psi}}(\delta) = \mp C_{Y'_{\psi}} \sin\delta_f \\
C_{Y'_{\psi}}(\delta) &= -C_{Z'_{\theta}}(\delta) = C_{Y'_{\psi}} \cos\delta_f \\
C_{Y'_{q'}}(\delta) &= -C_{Z'_{r'}}(\delta) = \mp C_{Y'_{q'}} \cos\delta_f \\
C_{Y'_{r'}}(\delta) &= -C_{Z'_{q'}}(\delta) = -C_{Y'_{q'}} \sin\delta_f \\
C_{m'_{\theta}}(\delta) &= C_{m'_{\psi}} \sin\delta_m \\
C_{m'_{\psi}}(\delta) &= \pm C_{m'_{\psi}} \cos\delta_m \\
C_{m'_{q'}}(\delta) &= C_{m'_{q'}} \cos\delta_m \\
C_{m'_{r'}}(\delta) &= \mp C_{m'_{q'}} \sin\delta_m \\
C_{n'_{\theta}}(\delta) &= -C_{m'_{\psi}}(\delta) = \mp C_{m'_{\psi}} \cos\delta_m \\
C_{n'_{\psi}}(\delta) &= C_{m'_{\theta}}(\delta) = C_{m'_{\psi}} \sin\delta_m \\
C_{n'_{q'}}(\delta) &= -C_{m'_{r'}}(\delta) = \pm C_{m'_{q'}} \sin\delta_m \\
C_{n'_{r'}}(\delta) &= C_{m'_{q'}}(\delta) = C_{m'_{q'}} \cos\delta_m
\end{aligned}
$$

Introduction

FORCES and moments generated by the propeller at an angle of attack or in yaw can have appreciable effect on the flying qualities of an airplane and (considering the cross-derivatives) on propeller whirl flutter. At high angles of attack they can strongly affect longitudinal stability, drag, tail effectiveness, and lift. In addition, side force and directional stability are involved. The use of highly loaded propellers of large solidity, characteristic of modern turboprop and tilting propeller VTOL aircraft, emphasizes the importance of readily available, accurate methods for predicting these forces and moments. For propellers at moderate angles of incidence, the theory is amply presented by Ribner,[1-3] where forces and moments for two representative blade shapes are given. In addition, experimental investigations[4] have been made of the characteristics of propellers at high incidence (in a range from 0° to 90°) in an attempt to attain some understanding of the phenomena involved.

The present study has been undertaken to evolve general force and moment expressions, which are valid for all propeller geometries at both moderate and high angles of incidence and which are sufficiently straightforward for use in handbook form.

Derivatives Due to Small Angles of Incidence

The procedure used for obtaining simplified theoretical relations of the characteristics of an inclined propeller is to first determine approximate equations of the propeller geometry and operating parameters from the analysis of Refs. 1 and 2 and second, to establish by statistical means the equation constants and possibly slightly altered functions from the computed data of given blade shapes.

Functional Approximation of Ribner's Analysis

Approximate values of the side force and moment equations are presented in the following forms in Ref. 2:

$$C_{Y'_{\psi}} \cong 1.14\sigma I_1 f \qquad C_{Y'_{q'}} \cong -(1 + a)\sigma I_2$$

$$C_{m'_{q'}} \cong -\tfrac{1}{2}(1 + a)\sigma I_3$$

To the same order of approximation, the pitching moment coefficient due to yaw can be approximated as

$$C_{m'_{\psi}} \cong 0.57\sigma I_2 f[1 + (2/\sigma I_2)J(2a/\pi)]$$

where the I's given in Ref. 2 are integrations along the blade chord and the sine or cosine of the blade pitch distribution. In the form of ratios to the side force derivative, a further simplification is made (assuming $f = 1 + a$)

$$\frac{C_{Y'_{q'}}}{C_{Y'_{\psi}}} \cong \frac{-I_2}{1.14I_1} \qquad \frac{C_{m'_{q'}}}{C_{Y'_{\psi}}} \cong \frac{-I_3}{2.28I_1}$$

$$\frac{C_{m'_{\psi}}}{C_{Y'_{\psi}}} \cong \frac{I_2}{2I_1}\left(1 + \frac{2}{\sigma I_2} J \frac{2a}{\pi}\right)$$

The blade pitch distribution can be approximated quite well by the function $\tan\beta_0 = 0.75 \tan\beta/r'$, where $r' = r/R$. Geometric pitch is given by $(p/D) = \pi r' \tan\beta_0$; thus the assumed blade pitch distribution is that having a constant geometric pitch along the blade. Most blades have a relatively constant geometric pitch, and all approximate an average at $r' = 0.75$.

The effect of blade chord distribution along the blade radius will be studied by examining a blade chord that is constant with r', $(\bar{b}'/b'_{0.75}) = 1$, and a blade that is strongly curved with a maximum at $r' = 0.5$, $(b'/b'_{0.75}) = 3.48$ $(\bar{b}'/b'_{0.75})$ $(r' - r'^3)$, where $(\bar{b}'/b'_{0.75}) = 0.876$. With the assumed blade pitch distribution, an approximate integration for I_1 leads to the same function, but with the constant 3.506 for the straight blade and 3.573 for the highly curved blade. An average of these two constants approximates the I_1 integral as

$$I_1 \cong 3.54(\bar{b}'/b'_{0.75}) \sin(\beta + 8)$$

Since factoring out the average chord leads to a constant factor (within ±1% of the mean for the two blades), the average chord can be considered as a primary blade parameter. A similar analysis for I_2 yields a constant that is ±3% from the mean constant, and I_2 is approximated by

$$I_2 \cong 2.03(\bar{b}'/b'_{0.75}) \cos(\beta + 3)$$

The integral I_3, which is independent of pitch distribution, is most easily approximated from Fig. 2 of Ref. 1 by

$$I_3 = [3/(J + 2\sigma_e)](\bar{b}'/b'_{0.75})$$

where σ_e introduces a new parameter defined as $\sigma_e = (\bar{b}'/b'_{0.75})\sigma$, an effective solidity value.

With the I's approximated, the force coefficient and the force and moment ratios can be evaluated as

$$C_{Y'_{\psi}} \cong 4.0\ \sigma_e \sin(\beta + 8) f \tag{1}$$

$$\frac{C_{m'_{\psi}}}{C_{Y'_{\psi}}} \cong 0.29 \frac{\cos(\beta + 3)}{\sin(\beta + 8)}\left[1 + \frac{J(2a/\pi)}{\sigma_e \cos(\beta + 3)}\right] \tag{2}$$

$$C_{Y'_{q'}}/C_{Y'_{\psi}} \cong -\cos(\beta + 3)/2 \sin(\beta + 8) \tag{3}$$

$$C_{m'_{q'}}/C_{Y'_{\psi}} \cong -3/[8(J + 2\sigma_e) \sin(\beta + 8)] \tag{4}$$

Equations (1–4) give the first-order approximation and an indication of the functional dependence. Since the pitching or yawing velocity forces and moments generated by the propeller contribute relatively little to the airplane, Eqs. (3) and (4) will be considered as final.

Statistical Evaluation of Side Force Slope (same as Normal Force Slope)

The thrust factor f in Eq. (1) is unity at thrust equal to zero. It is pointed out in Ref. 3 that factoring the thrust factor as in Eq. (1) leads to values within ±4% of those of a complete solution for high values of thrust. A more accurate equation of $C_{Y'_{\psi}}$ than that given by Eq. (1) remains to be evaluated.

In Ref. 3 charts of $C_{Y'_{\psi}}$ at zero thrust are presented for two blade shapes, two to six blades, and a blade pitch range from 15° to 55°. The blades are the Hamilton Standard 3155-6 with spinner [variable chord, maximum at $0.6R$ and $(\bar{b}'/b'_{0.75}) = 0.860$], and the NACA 10-3062-045 with spinner [almost constant chord with $(\bar{b}'/b'_{0.75}) = 0.974$].

These side force derivative values of Ref. 3 are here divided by $\sin(\beta + 8)$ for five values of β (15°, 25°, 35°, 45°, and 55°). The resulting five constants vary a maximum of ±2% from the mean value. This mean value according to Eq. (1) should depend only on σ_e. It was found, however, that four mean values, corresponding to four σ_e's, did not vary linearly

with σ_e, but by a slightly altered function. For the Hamilton blade, the four mean values are related accurately by $4.22\sigma_e/(1 + 2\sigma_e)$, whereas the analysis for the NACA blade leads to the value $4.28\sigma_e/(1 + 2\sigma_e)$, or essentially the same function. Since the results from two arbitrarily chosen different blade shapes lead to the same equation, the inference is that the equation is general for all blade shapes. The complete equation is the product of the parts that were divided out, or

$$C_{N'_{\alpha_{in}}} = C_{Y'_\psi} = [4.25\ \sigma_e/(1 + 2\sigma_e)]\sin(\beta + 8)f \quad (5)$$

A statistical evaluation of $C_{Y'_\psi}$ for the counter-rotating propeller gives an equation similar to Eq. (5):

$$C_{N'_{\alpha_{in}}} = C_{Y'_\psi} = [3.86\sigma_e/(1 + \sigma_e)]\sin(\beta + 14)f \quad (6)$$

Simplification of Thrust Factor

In Ref. 1 the thrust factor is presented as a function of the incremental slip-stream velocity at the propeller disk. By momentum theory, this velocity is $a = 0.5[(1 + T_c')^{1/2} - 1]$, which, when inserted in the thrust factor, leads to

$$f - 1 = \tfrac{1}{2}[(1 + T_{c'})^{1/2} - 1] + [T_{c'}/4(2 + T_{c'})] \quad (7)$$

By considering the limit conditions of f at T_c' near zero and infinity, a simplification leads to

$$f \cong 1 + 3T_{c'}/8(1 + \tfrac{2}{3}T_{c'})^{1/2} \quad (8)$$

which approaches a difference of 1.2% less than Eq. (7) at $T_c' = 20$.

Compressibility Effect

A first-order effect of compressibility is developed in Appendix B of Ref. 2. The Ref. 2 equation is very cumbersome but is duplicated here within ±2% by

$$M_{eff}/M = 1 + [\tfrac{8}{3}/(\tfrac{3}{2} + J)J] \quad (9)$$

The value of the compressible normal force derivative is then

$$C_{N'_{\alpha_{in_{comp}}}} = \frac{C_{N'_{\alpha_{in}}}}{(1 - \{1 + [\frac{8}{3}/(\frac{3}{2} + J)J]\}^2 M^2)^{1/2}} \quad (10)$$

Inflow Angle and Upwash Due to Wing, Fuselage, and Other Propellers

The inflow angle is

$$\alpha_{in} = \alpha - \epsilon_w - \epsilon_{fus} - \epsilon_{prop} + i_T = \left(1 - \frac{d\epsilon_w}{d\alpha} - \frac{d\epsilon_{fus}}{d\alpha} - \frac{d\epsilon_{prop}}{d\alpha}\right)\alpha + \alpha_{in_0} \quad (11)$$

where ϵ_{fus} and ϵ_{prop} have values for multipropeller airplanes and are zero for a single propeller mounted at the nose of a fuselage. The wing term $1 - d\epsilon_w/d\alpha$ is presented in Ref. 3 for three aspect ratios, based on elliptic loading. The following upwash factor is evaluated from Ref. 3:

$$1 - \frac{d\epsilon_w}{d\alpha} = 1 + \frac{2A}{9(A + 10)}\left(\frac{1}{(x_{L.75}/c_r) + \frac{1}{10}} + \frac{1}{(x_{R.75}/c_r) + \frac{1}{10}}\right) \quad (12)$$

where, since the wing leading edge is not always unswept, the $x_{L.75}$ represents the longitudinal distance from the left blade 0.75 radius point to the wing leading edge and $R.75$ similarly from the right side of the disk.

For propellers mounted on the wing, the fuselage creates an upwash at the propeller disk. This upwash will be approximated by that because of a falling cylinder at a velocity of $V(\alpha + \alpha_{fus_0})$. Then

$$\frac{d\epsilon_{fus}}{d\alpha} = -\frac{1}{2}\left[\left(\frac{R_{fus}}{y_{L.75}}\right)^2 + \left(\frac{R_{fus}}{y_{L.75}}\right)^2\right]$$

$$\epsilon_{fus_0} = -\frac{1}{2}\alpha_{fus_0}\left[\left(\frac{R_{fus}}{y_{L.75}}\right)^2 + \left(\frac{R_{fus}}{y_{R.75}}\right)^2\right] \quad (13)$$

where $y_{L.75}$ is the lateral distance from fuselage center to the left blade 0.75 radius point, and $y_{R.75}$ to the right side 0.75 radius point.

Similarly, a falling slip stream (at the propeller disk) gives

$$\frac{d\epsilon_{prop}}{d\alpha} = -\frac{1}{4}\sum_{other\ props}\left[\left(\frac{R}{\Delta y_{L.75}}\right)^2 + \left(\frac{R}{\Delta y_{R.75}}\right)^2\right]\frac{d\epsilon_{slip}}{d\alpha_{in}}\frac{d\alpha_{in}}{d\alpha} \quad (14)$$

$$\epsilon_{prop_0} = -\frac{1}{4}\sum_{other\ props}\left[\left(\frac{R}{\Delta y_{L.75}}\right)^2 + \left(\frac{R}{\Delta y_{R.75}}\right)^2\right]\frac{d\epsilon_{slip}}{d\alpha}\alpha_{in_0}$$

where $\Delta y_{L.75}$ is the lateral distance from one propeller axis to the other propeller left blade 0.75 radius point, and $\Delta y_{R.75}$ to the right side. This contribution has a significant value only when $\Delta y < 2R$ and can be neglected if a fuselage separates the propellers.

Average Blade Chord

The average blade chord is defined as

$$\bar{b}' = \frac{1}{0.8}\int_{0.2}^{1} b'dr'$$

A combination of Simpson's Rule and interpolation formula results in

$$b' = 0.16(\tfrac{5}{4}b'_{0.25} + 2b'_{0.50} + 2b'_{0.75} + b'_{0.95}) \quad (15)$$

This integration has proved to be accurate to 0.5% for six different blade shapes.

Statistical Evaluation of $C_{m'_\psi}/C_{Y'_\psi}$

The approximate relation given by Eq. (2) indicates that this moment derivative ratio can be evaluated in two parts; first, in a thrust equal to zero ($a = 0$) and second, in a thrust factor. In Ref. 3, data are presented of $C_{m'_\psi}$ at $T_{c'} = 0$ as a function of β for two solidity values for the Hamilton Standard 3155-6 blade. Values of $C_{m'_\psi}/C_{Y'_\psi}$ at $T_{c'} = 0$ were taken at $\beta = 15°, 25°, 35°, 45°$, and $55°$. The function that satisfied these data to within 1.5% is given by

$$\left(\frac{C_{m'_\psi}}{C_{Y'_\psi}}\right)_{T_{c'}=0} = \frac{0.321}{\sigma_e + \tan(\beta + 10)} \quad (16)$$

The term $J(2a/\pi)$ in the thrust factor of Eq. (2) requires evaluation as a function of thrust coefficient. From momentum consideration $2a/\pi = (1/\pi)[(1 + T_{c'})^{1/2} - 1]$. Based on eight different propellers, experimental data of C_T proportional to advance ratio for β from 15° to 60° statistically results in the following equations:

$$C_T = \frac{4.6\sigma_e\cos\beta}{1 + 3\sigma_e + (9\sigma_e/B)}(J_0 - J)$$

$$C_{T_{max}} \cong 2.2\sigma_e \quad (17)$$

$$J_0 = 2.2\tan(\beta + 5) \quad (18)$$

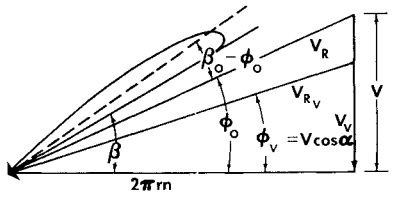

Fig. 1 Blade velocity for uninclined prop, for prop inclined at angle $\alpha = 0$, and blade in vertical position.

Using a typical value of σ_e in the denominator, $C_T = 2.9\ \sigma_e \cos\beta\ (J_0 - J)$; then $T_{c'} = 2.9(8/\pi)\sigma_e \cos\beta(J_0 - J)/J^2$. Solving for J in terms of $T_{c'}$, then combining with the $(2a/\pi)$ expression, and simplifying to an approximate function, results in

$$J\frac{2a}{\pi} \cong \frac{0.35\tan(\beta + 5)T_{c'}}{1 + 0.272[\tan(\beta + 5)/\sigma_e \cos\beta]^{1/2}T_{c'}} \quad (19)$$

Reference 3 presents plotted values of f_m (moment thrust factor) which, when divided by f, can be used to correct Eq. (19). Based on one blade shape and two solidities, the thrust factor of Eq. (2) is evolved to

$$1 + \frac{J(2a/\pi)}{\sigma_e \cos(\beta + 3)} = 1 + \frac{\frac{1}{3}(\tan\beta/\sigma_e \cos\beta)T_{c'}}{1 + \frac{3}{4}(\tan\beta/\sigma_e \cos\beta)^{1/2}T_{c'}} \quad (20)$$

The product of Eqs. (16) and (20) gives $C_{m'_\psi}/C_{Y'_\psi}$.

Damping-in-Roll Due to Propeller

For multipropeller airplanes, the normal force created by an antisymmetric inflow angle generated in rolling causes a countermoment or damping. Since the inflow angle is antisymmetric, the normal forces are antisymmetric for opposing propellers, or a countercouple is formed. For one propeller located laterally at y,

$$\text{rolling moment} = qC_{l'}S'D = qC_{N'_{\alpha_{in}}}y\{-(pb/2V)[y/(b/2)]\}S'$$

$$C_{l'_{p'}} = -\frac{1}{4}C_{N'_{\alpha_{in}}}\left[\left(\frac{y_{L.75}}{R}\right)^2 + \left(\frac{y_{R.75}}{R}\right)^2\right] \quad (21)$$

where $y_{L.75}$ represents the lateral distance from the airplane plane of symmetry to the left blade 0.75 radius point and $R.75$ to the right side. For two symmetrically mounted propellers this value is doubled.

Downwash or Sidewash in Slip Stream

The propeller at an angle of attack creates a lift due to thrust and normal force, and because of momentum conservation it must deflect a mass of air downward. For propellers operating near each other, this downwash must be known in order to predict the inflow angle accurately, as considered in Eq. (14). The induced flow in the slip stream (aft one propeller diameter or more) as predicted by theory[3] is

$$\frac{d\epsilon_{slip}}{d\alpha_{in}} = \frac{1 + T_{c'} - (1 - T_{c'})^{1/2}}{2 + T_{c'}} + \left[\frac{3 + 2T_{c'} + (1 + T_{c'})^{1/2}}{(2 + T_{c'})^2}\right]\frac{(1 + T_{c'})^{1/2}}{4}(C_{Y'_\psi})_{T_{c'}=0} \quad (22)$$

Within a close accuracy, Eq. (22) can be rewritten as

$$\frac{d\epsilon_{slip}}{d\alpha_{in}} \cong \frac{T_{c'}}{4 + \frac{8}{7}T_{c'}} + \frac{\left(C_{N'_{\alpha_{in}}}\right)_{T_{c'}=0}(1 + 1.3T_{c'})^{1/2}}{4 + 2T_{c'}} = \tfrac{1}{4}\left[\left(C_{N'_{\alpha_{in}}}\right)_{T_{c'}=0} + T_{c'} - \tfrac{1}{5}T_{c'}^2\right] \text{ for } T_{c'} < 2 \quad (23)$$

Thrust, Power, and Derivatives Due to High Angles of Inclination

The variation of propeller thrust and power, with propeller axis inclination, can be represented in general form by using ratios of the respective value at inclination to the value at zero inflow. The term "general form" implies that these ratios will be quasi-independent of propeller geometry such as blade shape, solidity, and pitch distribution. The ratios will be dependent on the propeller operation parameter of blade angle and advance ratio, since these depend on angle of inclination. Propeller normal force ratios can be formed by the ratio of normal force at high angles of inclination to the typically computed linear relation $(dN/d\alpha)_{\alpha=0}$.

Effect of Inclination on Thrust

A propeller at angle of inclination experiences an increased loading on the downgoing blade and a loss of loading on the upgoing blade. This loading change is the result of both an effective angle-of-attack change on the blade and a change of dynamic pressure. The blade in the vertical position has no change except for a sweep angle effect. These changes can be seen from the velocity vector diagrams of Figs. 1–3.

Defining advance ratio as $J = V/nD$ and $r' = r/R$, from the geometry of Figs. 1–3,

$$\left.\begin{aligned} \tan\phi_0 &= V/2\pi rn = J/\pi r' \\ \tan\phi_{DN} &= V\cos\alpha/(2\pi rn + V\sin\alpha) = J\cos\alpha/(\pi r' + J\sin\alpha) \\ \tan\phi_{UP} &= V\cos\alpha/(2\pi rn - V\sin\alpha) = J\cos\alpha/(\pi r' - J\sin\alpha) \end{aligned}\right\} \quad (24)$$

Quantitative Propeller Analysis

This analysis results in a functional evaluation of the thrust and power characteristics. It is presented in detail in Ref. 5 for small blade angle of attack as follows:

$$C_T = K\pi r'\sigma\cos\beta_0(J_{0T} - J) \quad (25)$$

$$J_{0T} = \pi r'\tan\beta_0[1 - (C_D/C_{L\alpha}\cos^2\beta_0)]$$

$$C_P = K(\pi r')^2\sigma\sin\beta_0(J_{0P} - J) \quad (26)$$

$$J_{0P} = \pi r'\tan\beta_0[1 + (C_D/C_{L\alpha}\sin^2\beta_0)]$$

where K is an empirical constant and r', in this case, is the blade radius position of the representative blade section (generally $r' = 0.70$ to 0.75).

Evaluation of Thrust Ratio

From Eqs. (25) the thrust is proportional to $q(J_{0T} - J)/J^2$. From quasi-steady principles, this term is also the thrust at a given time in the blade cycle, provided that J is taken at the corresponding position in the cycle. Since $J = \pi r'\tan\phi$,

$$T \propto [(J_{0T}/\pi r') - \tan\phi/\tan^2\phi]$$

where the angle φ varies throughout the cycle when the propeller axis is inclined. For a blade in the vertical position there is only a sweep angle effect on the loading. The integrated thrust per cycle can be approximated by assuming that the thrust varies harmonically with the cycle angle. Letting $T = A_0 + A_1\cos\theta + A_2\cos2\theta$, the integrated thrust is

$$T = \frac{1}{2\pi}\int_0^{2\pi}(A_0 + A_1\cos\theta + A_2\cos2\theta)d\theta = A_0$$

It remains to evaluate the coefficients. At $\theta = 0$, $T = T_{max}$ (i.e., when $\phi = \phi_{DN}$), $\theta = \pi/2$, $T = T_{ver}$; $\theta = \pi$, $T = T_{min}$ (i.e., when $\phi = \phi_{UP}$). With these values, a simultaneous solution for the A's results in

$$\left.\begin{aligned} A_0 &= \tfrac{1}{2}T_{ver} + \tfrac{1}{4}T_{max} + \tfrac{1}{4}T_{min} \\ A_1 &= \tfrac{1}{2}T_{max} - \tfrac{1}{2}T_{min} \\ A_2 &= T_{max} + \tfrac{1}{4}T_{min} - \tfrac{1}{2}T_{ver} \end{aligned}\right\} \quad 2 \text{ harmonic}$$

If the thrust varies only sinusoidally, then

$$\left.\begin{aligned} A_0 &= \tfrac{1}{2}(T_{\max} + T_{\min}) \\ A_1 &= \tfrac{1}{2}(T_{\max} - T_{\min}) \end{aligned}\right\} \text{ 1 harmonic}$$

The utilization of the two-harmonic solutions permits a full (aspect ratio = ∞) sweep correction on the vertical blade, whereas the one-harmonic solution allows no corrections. With Eq. (24) the integrated thrust for two harmonics is

$$T(\alpha, J\cos\alpha) \propto \frac{1}{2}\frac{\dfrac{J_{0T}}{\pi r'} - \dfrac{J\cos\alpha}{\pi r'}}{\left(\dfrac{J\cos\alpha}{\pi r'}\right)^2} + \frac{\dfrac{J_{0T}}{\pi r'} - \dfrac{J\cos\alpha/\pi r'}{1 + (J\cos\alpha/\pi r')\tan\alpha}}{4\left(\dfrac{J\cos\alpha/\pi r'}{1 + (J\cos\alpha/\pi r')\tan\alpha}\right)^2} + \frac{\dfrac{J_{0T}}{\pi r'} - \dfrac{J\cos\alpha/\pi r'}{1 - (J\cos\alpha/\pi r')\tan\alpha}}{4\left(\dfrac{J\cos\alpha/\pi r'}{1 - (J\cos\alpha/\pi r')\tan\alpha}\right)^2}$$

The thrust at zero angle of inclination, but with the velocity equal to $V\cos\alpha$, is proportional to

$$T(0, J\cos\alpha) \propto \frac{(J_{0T}/\pi r') - (J\cos\alpha/\pi r')}{(J\cos\alpha/\pi r')^2}$$

Dividing the first equation by the second (note that the proportionality constants are the same and divide out) to form a ratio, and simplifying, results in

$$\left[\frac{T(\alpha, J\cos\alpha)}{T(0, J\cos\alpha)}\right]_{2\text{ harmonic}} = 1 + \frac{1}{2}\frac{(J_{0T}/\pi r')^2(J\cos\alpha/J_{0T})^2\tan^2\alpha}{1 - (J\cos\alpha/J_{0T})}$$

For a one harmonic solution, the same procedure leads to the same ratio, except that the one-half is replaced by one. Since the two-harmonic solution involves taking a full ($A = \infty$) sweep effect on the blade in vertical position, whereas the one-harmonic solution neglects this, it will be assumed that the correct thrust ratio is a mean of these two variations of thrust. Then

$$\frac{T(\alpha, J\cos\alpha)}{T(0, J\cos\alpha)} = 1 + \frac{3}{4}\frac{(J_{0T}/\pi r')^2(J\cos\alpha/J_{0T})^2\tan^2\alpha}{1 - (J\cos\alpha/J_{0T})} \quad (27)$$

An approximate thrust ratio theory for $\alpha = 90°$ can be formulated from the helicopter theory of Ref. 6. This ratio is

$$\left[\frac{T(90, 0)}{T(0, 0)}\right]_{\text{hel}} = 1 + \frac{3}{2}\left(\frac{J}{\pi}\right)^2 \times \left\{1 + \frac{\sigma_e}{\tan\beta_0}\left[1 + \left(1 + \frac{2}{\sigma_e}\tan\beta_0\right)^{1/2}\right]\right\}\cos\beta_0 \quad (28)$$

For $\alpha = 90°$, Eq. (27) becomes (in general $r' = 0.7$)

$$T(90, 0)/T(0, 0) = 1 + [\tfrac{3}{2}(J/\pi)^2]$$

This equation differs from Eq. (28) only by the solidity term and $\cos\beta_0$. Thus, if the J^2 term of Eq. (27) is factored by this term, this equation will approach the correct limit as α goes to 90°. However, the solidity term must vanish as

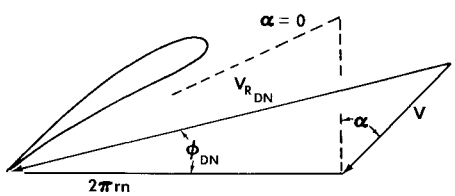

Fig. 2 Downgoing blade.

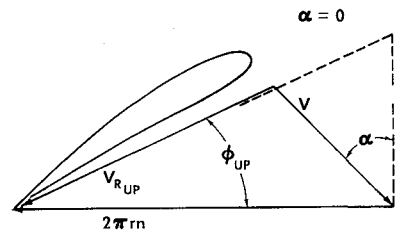

Fig. 3 Upgoing blade.

α approaches 0. The factor $(1 - \cos\alpha)$ will be used, since it decreases relatively linearly with α. Factoring the J^2 of Eq. (27) by $\{1 + (\sigma_e/\tan\beta_0)\,[1 + (1 + 2\tan\beta_0/\sigma_e)^{1/2}]\,(1 - \cos\alpha)\}\cos\beta_0$ and with $J_{0T} = \pi r'\tan\beta_0$, Eq. (27) results in

$$\frac{T(\alpha, J\cos\alpha)}{T(0, J\cos\alpha)} = 1 + \frac{3(J\cos\alpha/J_{0T})^2}{4[1 - (J\cos\alpha/J_{0T})]}\sin\beta_0(\tan\beta_0 + \sigma_e\{1 + [1 + (2/\sigma_e)\tan\beta_0]^{1/2}\}(1 - \cos\alpha)\tan^2)\alpha \quad (29)$$

Effect of Inclination on Power

Power is the rate of change of torque per unit time. Thus, the torque ratio is the same as the power ratio. From Eq. (26) the power will vary as

$$P \propto [(J_{0P}/\pi r) - \tan\phi]/\tan^2\phi \quad (30)$$

This is the same variation as that obtained for the thrust case. The power ratio has thus the same form as the thrust ratio of Eq. (29), except that J_{0T} is replaced by J_{0P}.

Approximation for J_{0P} and C_P

The advance ratio at zero power can be approximated in terms of J_{0T} by use of Eqs. (25) and (26), which indicate a function of the form

$$J_{0P} - J_{0T} = \pi r'(C_D/C_{L_\alpha})(1/\sin\beta_0\cos^3\beta_0)$$

Based on experimental data of eight different propellers, this difference is statistically approximated as

$$J_{0P} = J_{0T} + (16/\sin\beta_0\cos^4\beta_0)(\sigma_e/B)^2 \quad (31)$$

To the approximation of Eq. (17) it is seen from experimental data that the C_P can be represented as

$$C_P = [10.4\sigma_e\sin\beta_0/(1 + \sigma_e + 24\sigma_e/B)](J_{0P} - J) \quad (32)$$

Effect of High Inclination on the Derivatives

Normal force will be considered as proportional to the torque difference due to angle of inclination on the downgoing blade minus the torque difference on the upgoing blade. The torque is

$$Q \propto \{\sin\beta_0[(J_{0P}/\pi r') - \tan\phi]/(\tan^2\phi)\}q$$

Denoting Q_{0_α} as the constant torque at zero inclination, but operating with the effective velocity $V\cos\alpha$ or $J\cos\alpha$, the normal force is proportional to

$$N \propto (Q_{\alpha_{DN}} - Q_{0_\alpha}) - (Q_{\alpha_{UP}} - Q_{0_\alpha})$$

Applying Eqs. (24) leads to

$$N \propto 2\sin\beta_0\, q[(2J_{0P}/J\cos\alpha) - 1]\tan\alpha \quad (33)$$

Maintaining $V\cos\alpha$ as the effective velocity

$$(dN/d\alpha)_{\alpha=0} \propto 2\sin\beta_0 q[(2J_{0P}/J\cos\alpha) - 1]$$

The ratio of N at high α to the N of linear α is

$$\frac{N(\alpha, J\cos\alpha)}{dN(0, J\cos\alpha)/d\alpha} = \tan\alpha \quad (34)$$

The denominator values are readily available in the form

of $C_{N'_{\alpha in}}$; however, the J or thrust in $C_{N'_{\alpha in}}$ must be taken as $J\cos\alpha$ and velocity as $V\cos\alpha$.

Yaw Moment

Yaw moment due to angle of inclination will be considered as proportional to the thrust moment of the downgoing blade minus the thrust moment of the upgoing blade. This leads to

$$n \propto 2r'\cos\beta_0 q[(2J_{0T}/J\cos\alpha) - 1]\tan\alpha \tag{35}$$

The ratio of n at high α to the n of linear α is

$$\frac{n(\alpha, J\cos\alpha)}{dn(0, J\cos\alpha)/d\alpha} = \tan\alpha \tag{36}$$

Pitching

At an angle of inclination and with a pitching velocity q, the normal to the disk velocity on the top blade is $V\cos\alpha + r'Rq$ and on the bottom blade is $V\cos\alpha - r'Rq$. Defining $q' = qD/2V$, the $\tan\phi$ values are

$$\tan\phi_{\text{top}} = (J\cos\alpha/\pi r')[1 + (r'q'/\cos\alpha)]$$

$$\tan\phi_{\text{bot}} = (J\cos\alpha/\pi r')[1 - (r'q'/\cos\alpha)]$$

This angle differential causes a side force and a pitching moment. The side force is (assume $r' = 0.707$)

$$Y \propto Q_{\alpha_{\text{top}}} - Q_{\alpha_{\text{bot}}} \propto -\pi\sin\beta_0 \times (2J_{0P}/\{J^2[1 - (q'^2/2\cos^2\alpha)]^2\cos^2\alpha\} + 1/\{J[1 - (q'^2/2\cos^2\alpha)]\cos\alpha\})(q'/\cos\alpha)$$

Maintaining $V[1 - (q'^2/2\cos^2\alpha)]\cos\alpha$ as the effective velocity, the ratio at high α becomes

$$\frac{Y\{q', \alpha, J[1 - (q'^2/2\cos^2\alpha)]\cos\alpha\}}{dY\{0, 0, J[1 - (q'^2/2\cos^2\alpha)]\cos\alpha\}/dq'} = \frac{q'}{\cos\alpha} \tag{37}$$

Similarly, the pitching moment ratio is

$$\frac{m\{q', \alpha, J[1 - (q'^2/2\cos^2\alpha)]\cos\alpha\}}{dm\{0, 0, J[1 - (q'^2/2\cos\alpha)]\cos\alpha\}/dq'} = \frac{q'}{\cos\alpha} \tag{38}$$

Thus, the side force and pitching moment due to pitching velocity can be estimated from small angle derivatives, but with velocity and advance ratio taken as $[1 - (q'^2/2\cos^2\alpha)]V\cos\alpha$ and $[1 - (q'^2/2\cos^2\alpha)]J\cos\alpha$.

Other Considerations

Estimation of Phase Angle

As can be seen in Figs. 1–3, the propeller at inclination has a variation of blade angle of attack and dynamic pressure during a cycle. Thus, in a cycle, the lift builds up and decreases in a harmonic fashion and appears as unsteady motion. As angle of attack increases, circulation increases, and a starting vortex is shed which induces a downwash and changes the build-up of circulation. Unsteady motion in general causes the lift cycle to be out of phase with the angle-of-attack cycle. Propeller forces and moments would then have a component in both the lateral and vertical directions. For example, the normal force due to angle of inclination would then develop a side force equal to the product of the normal force and sine of the phase angle, and normal force is the product of normal force computed at zero-phase angle and the cosine of the phase angle.

An approximation of the propeller phase angle change can be obtained from an analogous wing unsteady solution. The assumption is made that the propeller forces and blade angle of attack are analogous to the lift of a wing that is harmonically pitching about the wing quarter-chord line.

Harmonic motion due to pure pitch is considered by several theories. In Ref. 7, p. 216, a prediction of phase angle is presented for infinite aspect-ratio wing based on Theodorsen's theory. In Ref. 8, p. 45, two low-aspect-ratio theories are compared; these methods are based on the works of Reissner and Lawrence-Gerber. These methods[7–8] lead to somewhat similar values, which indicate that aspect ratio has little influence on phase angle. The method that will be used is the Reissner averaged with the Lawrence-Gerber. These average values are then used to develop an arc-tangent function derived statistically as

$$\delta \cong 0.825\tan^{-1}2.027k \tag{39}$$

where δ is the phase angle and k the reduced frequency. Equation (39) is as accurate as the values that can be read from the chart in Ref. 8.

It remains to relate the reduced frequency to the advance ratio. This is somewhat complicated because the propeller forces are not solely related to freestream velocity as is wing lift. The reduced frequency is

$$k = \frac{\omega b'}{2V_{\text{effective}}} = \frac{\pi(\bar{b}'/D)}{(V/nd)_{\text{effective}}}$$

Lift on a wing is proportional to V^2. However, Eqs. (33) and (35) show propeller forces and moments proportional to velocity as

$$N \propto V^2[(2J_{0P}/J) - 1] \qquad n \propto V^2[(2J_{0T}/J) - 1]$$

In analogy to the wing, the effective velocities will be taken as the square root of these terms. With $(\bar{b}'/D) = (3\pi\sigma_e/4B)$ the phase angles from Eq. (39) then are

$$\delta_f = 0.825\tan^{-1}[15\sigma_e/B(2J_{0P}J - J^2)^{1/2}] \tag{40}$$

$$\delta_m = 0.825\tan^{-1}[15\sigma_e/B(2J_{0T}J - J^2)]^{1/2} \tag{41}$$

where δ_f is the phase angle for propeller forces and δ_m the phase angle for propeller moments.

Section Lift-Curve Slope Correction

The theory has assumed a section lift-curve slope of (0.95) 2π/rad for the blade. For values other than this, the effective solidity can be factored (similar to aspect ratio in wing theory) by the ratio of a_0 to $(0.95)2\pi$. Thus, the solidity parameter becomes

$$\sigma_e = [a_0/(0.95)2\pi](\bar{b}'/b'_{0.75})\sigma \tag{42}$$

where a_0 is the section lift-curve slope of the blade.

Blade Pitch Angle Reference

The blade pitch angle β appearing in the equations throughout the report are for a reference β that differs by 5° from the blade angle for zero lift. For a typical propeller blade this difference is normally about 5°. However, if this difference is not 5°, then the pitch angle to be used is

$$\beta = \beta_{\text{ref}} - (\beta_{C_l=0} + 5°) \tag{43}$$

where all β's are measured at the 0.75 radius blade station, and β_{ref} (at $c_l = 0$) is the blade reference angle at which lift equals zero (normally about −5°). For a symmetric section, β_{ref} (at $c_l = 0$) equals 0°; then $\beta = \beta_{\text{ref}} - 5°$. For a highly cambered or flapped section β_{ref} (at $c_l = 0$) could be −10°; then $\beta = \beta_{\text{ref}} + 5°$.

Use and Correlation of Method

All final equations are tabulated in Table 1 for convenience. In practice, knowing the airplane configuration, only Table 1 and the Nomenclature section are needed for evaluation of all inclined propeller characteristics.

Table I Characteristics of an inclined propellar

Symbol	Function (per radian and per propellar)[a]	Eq. or Ref.
$C_{N'_{\alpha_{in}}}$ or $C_{Y'_{\psi}}$	$\frac{4.25\sigma_e}{1+2\sigma_e}\sin(\beta+8)\left(1+\frac{3T_{c'}}{8(1+\frac{2}{3}T_{c'})^{1/2}}\right)$	(5) and (8)
$(C_{N'_{\alpha_{in}}}$ or $C_{Y'_{\psi}})$ counter-rotation	$\frac{3.86\sigma_e}{1+\sigma_e}\sin(\beta+14)\left(1+\frac{3T_{c'}}{8(1+\frac{2}{3}T_{c'})^{1/2}}\right)$	(6) and (8)
$\frac{C_{n'_{\alpha_{in}}}}{C_{N'_{\alpha_{in}}}}$ or $\frac{C_{m'_{\psi}}}{C_{Y'_{\psi}}}$	$\frac{0.321}{\sigma_e+\tan(\beta+10)}\left(1+\frac{\frac{1}{3}(\tan\beta/\sigma_e\cos\beta)T_{c'}}{1+\frac{3}{4}(\tan\beta/\sigma_e\cos\beta)^{1/2}T_{c'}}\right)$	(16) and (20)
$\frac{C_{N'_{r'}}}{C_{N'_{\alpha_{in}}}}$ or $\frac{C_{Y'_{q'}}}{C_{Y'_{\psi}}}$	$\frac{-\cos(\beta+3)}{2\sin(\beta+8)}$	(3)
$\frac{C_{n'_{r'}}}{C_{N'_{\alpha_{in}}}}$ or $\frac{C_{m'_{q'}}}{C_{Y'_{\psi}}}$	$\frac{-3}{8(J+2\sigma_e)\sin(\beta+8)}$	(4)
$C_{l'_{p'}}$	$-\frac{1}{4}C_{N'_{\alpha_{in}}}\left[\left(\frac{y_{L.75}}{R}\right)^2+\left(\frac{y_{R.75}}{R}\right)^2\right]$	(21)
$(C_{N'_{\alpha_{in}}}$ or $C_{Y'_{\psi}})_{\text{compressible}}$	$C_{N'_{\alpha_{in}}}\Big/\left(1-\left[1+\frac{\frac{8}{3}}{(\frac{3}{2}+J)J}\right]^2M^2\right)^{1/2}$	(10)
δ_f, δ_m	$\delta_f=0.82\tan^{-1}\frac{15\sigma_e}{B(2J_{0P}J-J^2)^{1/2}}$ $\quad$ $\delta_m=0.82\tan^{-1}\frac{15\sigma_e}{B(2J_{0T}J-J^2)^{1/2}}$	(40) and (41)
α_{in}	$\dfrac{\alpha+\frac{2A\alpha}{9(A+10)}\left(\frac{1}{(x_{L.75}/c_r)+\frac{1}{10}}+\frac{1}{(x_{R.75}/c_r)+\frac{1}{10}}\right)+i_T+\frac{1}{2}(\alpha_{fus0}+\alpha)\left[\left(\frac{R_{fus}}{y_{L.75}}\right)^2+\left(\frac{R_{fus}}{y_{R.75}}\right)^2\right]}{1-\frac{1}{4}\sum\left[\left(\frac{R}{\Delta y_{L.75}}\right)^2+\left(\frac{R}{\Delta y_{R.75}}\right)^2\right]\frac{d\epsilon_{slip}}{d\alpha_{in}}}$	(11–14)
$\frac{d\epsilon_{z_{slip}}}{d\alpha_{in}}$ or $\frac{d\epsilon_{v_{slip}}}{d\psi}$ (inside slip stream)	$\frac{1}{4}\left[\left(C_{N'_{\alpha_{in}}}\right)_{T_{c'}=0}+T_{c'}-\frac{1}{5}T_{c'^2}\right]T_{c'}<2$	(23)
σ_e	$\frac{\bar{b}'}{b'_{0.75}}\sigma=\frac{\bar{b}'}{b'_{0.75}}\left(\frac{4B}{3\pi}\frac{b'_{0.75}}{D}\right)$, or $\frac{a_0}{2\pi(0.95)}\frac{\bar{b}'}{b'_{0.75}}\sigma$	(42)
$\bar{b}'$	$\frac{1}{0.8}\int_{0.2}^{1}b'dr'=0.16\left(\frac{5}{4}b'_{0.25}+2b'_{0.50}+2b'_{0.75}+b'_{0.95}\right)$	(15)
J_{0T}, J_{0P}	$J_{0T}=2.2\tan(\beta+5)$ $J_{0P}=J_{0T}+\frac{16}{\sin\beta_0\cos^4\beta_0}\left(\frac{\sigma_e}{B}\right)^2$	(18) and (31)
C_T or $\frac{\pi J^2}{8}T_{c'}$, C_P	$C_T=\frac{4.6\sigma_e\cos\beta}{1+3\sigma_e+(9\sigma_e/B)}(J_{0T}-J)$, $C_{T_{max}}\cong 2.2\sigma_e$ $C_P=\frac{10.4\sigma_e\sin\beta_0}{1+\sigma_e+(24\sigma_e/B)}(J_{0P}-J)$	(17) and (32)
ΔC_{mP}	$\frac{S'}{S}\left[\frac{z}{\bar{c}}T_{c'}+C_{N'_{\alpha_{in}}}\alpha_{in}\frac{l_1}{\bar{c}}\right]$	Ref. 3
	$\frac{S'}{S}\left(\frac{z}{\bar{c}}\frac{dT_{c'}}{dC_L}+\frac{l_1}{\bar{c}}\frac{C_{N'_{\alpha_{in}}}}{C_{L_{\alpha P}}}\frac{d\alpha_{in}}{d\alpha}\right)$[gives change in neutral point]	
$\frac{\Delta x}{\bar{c}}=\frac{d(\Delta C_{mP})}{d(C_L)}$	$\frac{S'}{S}\frac{l_1}{\bar{c}}\frac{C_{N'_{\alpha_{in}}}}{C_{L_{\alpha P}}}\frac{d\alpha_{in}}{d\alpha}$ [gives change in a.c.]	Ref. 3
ΔC_{nP}	$\frac{S'}{S}\left[C_{Y'_{\psi}}\frac{l_1}{b}\psi-C_{n'_{\alpha_{in}}}\alpha_{in}\frac{D}{b}\right]$	Ref. 3
$\frac{C_T(\alpha,\ J\cos\alpha)}{C_T(0,\ J\cos\alpha)}$	$1+\frac{3(J\cos\alpha/J_{0T})^2}{4[1-(J\cos\alpha/J_{0T})]}\sin(\beta+5)(\tan(\beta+5)+\sigma_e\{1+[1+(2/\sigma_e)\tan(\beta+5)]^{1/2}\}(1-\cos\alpha))\tan^2\alpha$	(29)
$\frac{C_P(\alpha,\ J\cos\alpha)}{C_P(0,\ J\cos\alpha)}$	$1+\frac{3(J\cos\alpha/J_{0P})^2}{4[1-(J\cos\alpha/J_{0P})]}\sin(\beta+5)(\tan(\beta+5)+\sigma_e\{1+[1+(2/\sigma_e)\tan(\beta+5)]^{1/2}\}(1-\cos\alpha))\tan^2\alpha$	(30)
	$\frac{C_N(\alpha,\ J\cos\alpha)}{C_{N_\alpha}(0,\ J\cos\alpha)}=\frac{C_n(\alpha,\ J\cos\alpha)}{C_{n_\alpha}(0,\ J\cos\alpha)}=\tan\alpha$	(34) and (36)
	$\frac{C_Y\{q',\ \alpha,\ J[1-(q'^2/2\cos^2\alpha)]\cos\alpha\}}{C_{Y_{q'}}\{0,\ 0,\ J[1-(q'^2/2\cos^2\alpha)]\cos\alpha\}}=\frac{C_m\{q',\ \alpha,\ J[1-(q'^2/2\cos^2\alpha)]\cos\alpha\}}{C_{m_{q'}}\{0,\ 0,\ J[1-(q'^2/2\cos^2\alpha)]\cos\alpha\}}=\frac{q'}{\cos\alpha}$	(37) and (38)

[a] See Nomenclature for phase angle correction.

Correlation of Normal Force Derivative with Theory of Ref. 3 and Experiment

Reference 3 presents complete charts of $C_{N'_{\alpha_{in}}}$ derivatives for two blade shapes. The blades are the Hamilton Standard 3155-6 with spinner [variable chord with maximum at $0.6R$, $(\bar{b}'/b'_{0.75}) = 0.860$] and the NACA 10-3062-045 with spinner [almost constant chord, $(\bar{b}'/b'_{0.75}) = 0.974$]. For comparison with the $C_{N'_{\alpha_{in}}}$ value of Table 1, 44 values were taken from the reference charts for a range of nine solidity values (0.061 to 0.248), five values of pitch angle (15° to 55°), two, three, four, and six blades, and also counter-rotating propellers. In this 44-values correlation, the averaged difference was 0, the averaged absolute difference was 0.94%, and the maximum difference was ±2.7%.

Reference 3 presents a side force factor chart for interpolating values of C_{N_α} for other blade shapes in terms of the two blades described previously. The average of the side force factor chart values as compared with the $C_{N'_\alpha}$ of Table 1 is 0.278 and 0.277, respectively, for a constant chord ($\sigma_e = 0.185$) four-bladed propeller, and 0.161 and 0.164, respectively, for the Hamilton Standard 7125-6 ($\sigma_e = 0.106$) three-bladed propeller.

Experimental data of a complete airplane model showed $C_{N'_\alpha} = 0.481$ at $T_{c'} = 0$ and $C_{N_{\alpha'}} = 0.548$ at $T_{c'} = 0.5$. Calculating $C_{N'_\alpha}$ from Table 1 led to values 4.3 and 3.3% less than the experimental values, respectively. It should be noted that $C_{N'_\alpha} = C_{N'_{\alpha_{in}}} d\alpha_{in}/d\alpha$. For this airplane, $(d\alpha_{in}/d\alpha) = 1.583$, showing that almost 60% of the inflow at the propeller is due to the wing and fuselage.

Thrust, Power, and Derivative Correlation with Experiment to $\alpha = 85°$

A rather complete propeller test of three propellers at nine angles of incidence, ranging from 0° to 85°, is presented in Ref. 4. Thrust, power, and other forces and moments are plotted as a function of modified advance ratio ($J\cos\alpha$) for ten blade angles. The propellers were full scale and were tested in the Ames 40- × 80-ft wind tunnel. The data of propeller 1 were extensive, propeller 2 limited, and propeller 3 more limited (blades were hinged). Only the data of propellers 1 and 2 are used in the present correlation. The propeller geometries are as follows. For propeller 1: $B = 3$ blades, $D = 12$ ft, $b_{0.75'} = 1.17$ ft., $\sigma = 0.124$, $\sigma_e = 0.117$, and blade chord increases to $0.50R$, and is constant from $0.50R$ out. For propeller 2: $B = 3$ blades, $D = 10$ ft, $b_{0.75'} = 0.144$ ft, $\sigma = 0.183$, $\sigma_e = 0.186$, and blade chord is constant to $0.60R$, and decreases from $0.60R$ out. No tunnel corrections were made. Maximum variation of data points was ±8% from a faired line.

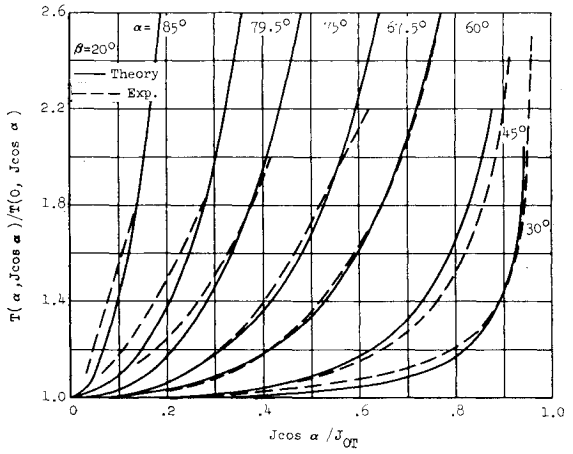

Fig. 4 Comparison of theoretical with experimental[4] thrust ratios. Propeller 1, $\sigma_e = 0.117$.

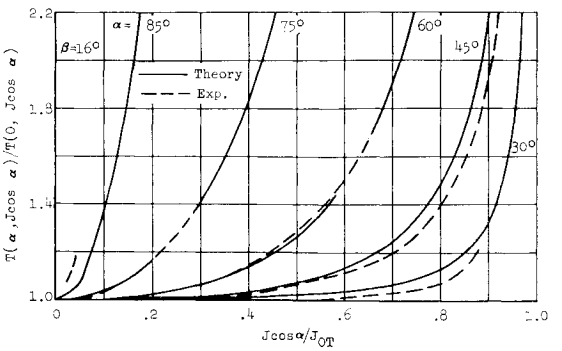

Fig. 5 Comparison of theoretical with experimental[4] thrust ratios. Propeller 2, $\sigma_e = 0.186$.

Figure 4 presents a thrust ratio correlation of an experiment from Ref. 4 and the theory as computed from Table 1. This correlation for $\beta = 20°$ is representative of correlations made at $\beta = 4°$, 12°, 16°, 20°, 30°, 35°, and 40°, and is presented in Ref. 10. Propeller 2 has a solidity substantially larger than propeller 1, and the thrust ratio is experimentally and theoretically larger as shown in Fig. 5. Figure 5 with $\beta = 16°$ is representative of correlations made at $\beta = 4°$, 12°, 16°, and 20°. The effect of β is to shift the family of curves slowly to the left as β increases.

In Fig. 6, the correlation between experimental power ratio with experimental thrust ratio is shown, and indicates that the power ratio has, in essence, the same function as the thrust ratio as predicted by theory. Figure 6 with $\beta = 30°$ is representative of correlations made at $\beta = 16°$, 20°, 30°, 35°, and 40°. At low β values, the power ratio curves appear somewhat erratic.

The normal force ratio as presented in Table 1 is compared with experimental data in Fig. 7. The data are presented as a function of angle of attack, and the variation with the tangent of the angle of attack is verified. The same type of correlation was made with the yaw moment ratio resulting in almost identical curves as in Fig. 7.

Figure 8 includes experimental force and moment phase angles from Ref. 9. These were for a windmilling propeller ($J = J_{0P}$) and measured C_{N_α}, C_{N_ψ}, C_{m_α}, and C_{m_ψ}. The angles are taken as $\delta_f = \tan^{-1} C_{N_\alpha}/C_{N_\psi}$, and $\delta_m = \tan^{-1} C_{m_\alpha}/C_{m_\psi}$. This propeller was four-bladed with $\sigma_e = 0.179$. Moment phase angles are also presented from Ref. 4, from which $\delta_m = \tan^{-1} C_{m_\alpha}/C_{n_\alpha}$. The theoretical phase angles, from the phase equations of Table 1, are compared with the corresponding experimental data. As can be seen, the data of Ref. 4 indicate a strong variation of phase angle with advance ratio at zero thrust, whereas Ref. 9 data show a milder variation. The theory lies between the two.

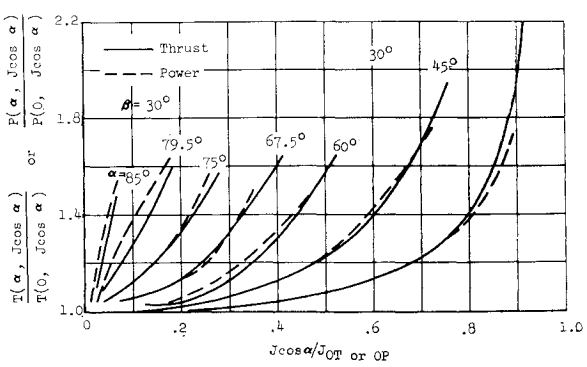

Fig. 6 Comparison of experimental[4] thrust with power ratios. Propeller 1.

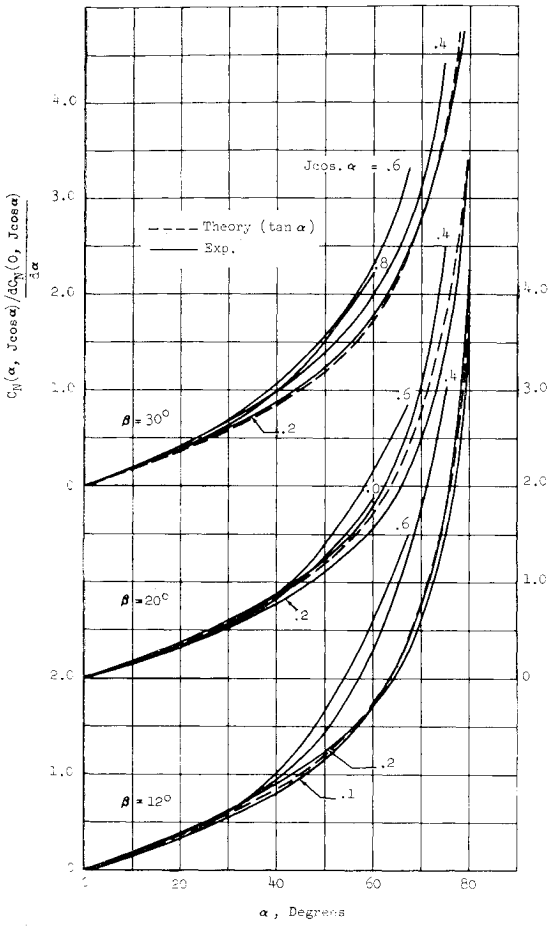

Fig. 7 Variation of experimental[1] normal force ratio with propeller angle of inclination. Propeller 1.

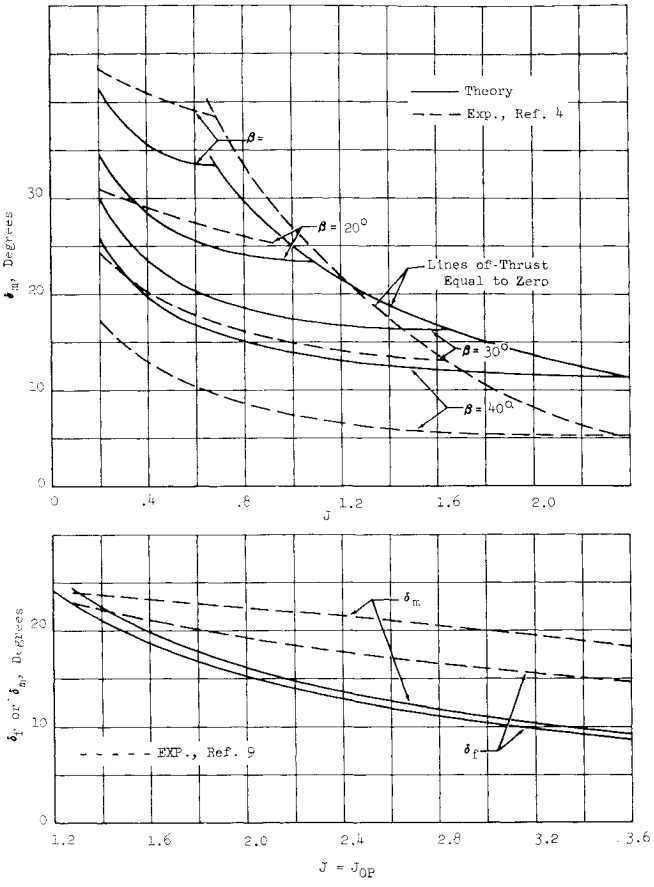

Fig. 8 Comparison of theoretical and experimental[4,9] phase angle.

Tunnel Wall Effect

The theoretical thrust ratios are consistently smaller than the experimental ratios at high angles of incidence (see Fig. 4). It can be suspected that at high angles of attack the flow is altered by the tunnel; that is, the tunnel floor and ceiling tend to keep the flow horizontal and thus the propeller senses a higher angle of attack than in free air. A partial estimate of the tunnel wall induced angle can be made by assuming that the propeller disk acts as a wing. For a wing, a typical correction is $\Delta\alpha = 0.125(S/C)C_L$ where C is the tunnel cross-sectional area and S the wing area. For the propeller, the projected area is $S = S' \sin\alpha$. The lift coefficient can be approximated by relating wing trailing vortex sheet downwash with the downwash in the slip stream due to a propeller. For a typical wing $d\epsilon/d\alpha = C_{L_\alpha}/2\pi A$ is equated to $d\epsilon_{slip}/d\alpha$. With the aspect ratio given by $4R^2/S' \sin\alpha$, then the lift coefficient is $C_L = 8\, d\epsilon_{slip}/d\alpha$, and the tunnel correction becomes $\Delta\alpha = (S'/C)\ (d\epsilon_{slip}/d\alpha)\ \sin\alpha$. The slip-stream downwash (for high $T_{c'}$) can be calculated from Eq. (22) in which $T_{c'}$ is determined from Table 1. Now as α approaches 90°, $T_{c'}$ approaches ∞, and the slip-stream downwash derivative approaches unity. For this limit, $\Delta\alpha = 2.28°$ $(S'/C = 0.040)$. Thus, if at low absissa values and at high α, the curves of Figs. 4 and 5 are moved to the left about 2°, the correlation would be improved. At a low angle of attack $\Delta\alpha$ becomes insignificant.

Propeller Shaft Load

The forces and moments as predicted by the equations of Table 1 are net values, that is, time averaged or resulting from an integration through a propeller cycle. The propeller shaft, with a single blade, senses a maximum and a minimum load twice during a cycle; with several blades, several extremes, but of lesser intensity depending on blade location, are sensed; with infinite blades, the shaft load is constant throughout the cycle. The airplane senses the net force or moment, as predicted from Table 1, whereas the cyclic variation of force appears as a vibration. It has probably been noted that the net load equations are independent of the number of blades (it only appears as a scalar factor in the solidity). The vibration effect is, however, as noted, very dependent upon the number of blades. The magnitude and blade dependency of the oscillatory part of the force can be visualized by considering that the force, for example, normal force, varies approximately as the absolute values of the sine of the cycle angle. A one-bladed propeller then creates a shaft force for which the minimum value is 100% less than the maximum; with two blades it is also 100% less; with three blades, a drop to 13.4% less; with four blades it goes back up to 29.3% less; with five blades it is 4.9% less; and with six blades it is 13.4% less. Thus, the magnitude of the vibratory part of the force at the propeller shaft is much stronger for the even-bladed than for the odd-bladed propeller. For the same solidity the net force of both is the same. The vibration advantages of odd-number blades is a consideration when a propeller is to operate at an inclined attitude.

Conclusions

Inclined force and moment equations have been developed in a relatively simple form covering the range of angle of attack from 0° to 90°. Use of a solidity based on average blade chord makes these equations valid for arbitrary blade shape. For obtaining absolute values from the thrust and

power ratios at high incidence, it is recommended that precalculated or tested propeller data for the zero angle-of-incidence values be used. If calculated or test thrust and power data is unavailable, use can be made of the zero incidence thrust and power equations presented. Comparison with experiment shows an engineering accuracy sufficient for establishing design criteria, trending studies, and preliminary configuration development, and performance estimates. All these results are applicable for propellers operating at high incidence or in large upflow and are thus applicable to VTOL-type operation as well as for conventional propeller operation.

References

[1] Ribner, H. S., "Formulas for propellers in yaw and charts of the side-force derivative," NACA Rept. 819 (1943).

[2] Ribner, H. S., "Propellers in yaw," NACA Rept. 820 (1943).

[3] Ribner, H. S., "Notes on the propeller and slip stream in relation to stability," NACA ARR L4I12a (WR L-25).

[4] Yaggy, P. F. and Rogallo, V. L., "A wind tunnel investigation of three propellers through an angle-of-attack range from 0° to 85°," NASA TN D-318 (May 1960).

[5] Von Mises, R., *Theory of Flight* (Dover Publications, Inc., New York, 1959), Chap. XI, pp. 302–309.

[6] Gessow, A. and Myers, G. P., *Aerodynamics of the Helicopter* (The Macmillan Co., New York, 1952), Chap. 8, p. 190.

[7] Fung, Y. C., *The Theory of Aeroelasticity* (John Wiley and Sons, Inc., New York, 1955), Chap. 6, p. 216.

[8] *Aeroelasticity Symposium, Gottingen, April 16–17, 1957*, NASA TT F-81, p. 45 (September 1963).

[9] Bland, S. R. and Bennett, R. M., "Wind-tunnel measurement of propeller whirl-flutter speeds and static-stability derivatives and comparison with theory," NASA TN D-1807 (August 1963).

[10] De Young, J., "Force and moment derivatives due to propellers of arbitrary configuration inclined with respect to freestream," AIAA Preprint 64-169 (1964).

MAY-JUNE 1965 J. AIRCRAFT VOL. 2, NO. 3

An Application of Hydropneumatic Propulsion to Hydrofoil Craft

JOHN D. PIERSON*
Martin Company, Baltimore, Md.

The design of large, high-speed hydrofoil craft is dependent upon the development of reliable and efficient means of converting very high power levels to effective thrust. A novel means has been developed which uses compressed air directly to produce thrust in an underwater, ramjet-like cycle: the MARJET hydrofoil, an integrated lifting propulsive system. The theory of operation is briefly reviewed, and the practical problems of incomplete mixing and heat transfer are discussed. Experimental data are presented to confirm the analysis and provide correlation factors for design use. Basic design charts for the internal performance of the MARJET and the related foil drag are presented, along with a recommended procedure for optimization of an integrated MARJET-hydrofoil design. A sample application to a large 80-knot hydrofoil craft shows that performance competitive with that forecast for supercavitating propellers would require multistage air compression with intercooling to approach isothermal conditions. However, used as a booster system, the MARJET will provide flexible and efficient high-speed thrust augmentation even with conventional turbocompressors for the air supply.

Introduction

THE design of large, high-speed hydrofoil craft requires a practical means of converting high power levels to thrust efficiently. Gas turbines can provide the necessary power at reasonable installed weight, but structural and arrangement problems make the conversion of the shaft power to thrust a real challenge to the designer. Developments in supercavitating propellers, high-speed gearing, pumps, and associated systems are extending the range of thrust production, but further growth in this direction may be limited by poor service life at high stress levels.

A propulsion system that uses compressed air as the power transmission medium, with direct conversion to thrust in a hydrodynamic ramjet, has been under development at the Martin Company for several years. Called MARJET, this system is inherently rugged and capable of large power conversion in vehicles moving through the water at high speed. Although MARJET may be pertinent to many fields of marine propulsion, the most recent development work has been directed toward its application to high-speed hydrofoil craft with the support of the Machinery Design Branch, Bureau of Ships.[1, 2]

An artist's concept of a MARJET-hydrofoil design is shown in Fig. 1. The basic powerplant (contained within the hull) consists of several engine-compressor units. The air from the compressors may be ducted together and distributed to the several foils through air passages within the struts and foils. The flexibility in design and the simplicity of the air power distribution and control are the prime advantages of the MARJET system.[1, 4] The question that remains, how well the air power can be converted to thrust, is the subject of this paper.

The combined MARJET hydrofoil is an integrated lifting propulsive system. The MARJET is incorporated within the lifting surface by splitting the normal foil shape and separating upper and lower surfaces to form the internal duct

Presented as Preprint 64-305 at the 1st AIAA Annual Meeting, Washington, D. C., June 29–July 2, 1964; revision received November 23, 1964. Work supported by Machinery Design Branch, Bureau of Ships.

* Senior Staff Engineer.